

A model-based Gait Recognition Method based on Gait Graph Convolutional Networks and Joints Relationship Pyramid Mapping

Na Li¹, Xinbo Zhao^{1*}, Chong Ma²

1. National Engineering Laboratory for Integrated Aero-Space-Ground-Ocean Big Data Application Technology, School of Computer Science, Northwestern Polytechnical University, China
2. School of Automation, Northwestern Polytechnical University, China

Abstract—Gait, as a unique biometric feature that can be recognized at a distance, which can be widely applied in public security. In this paper, we propose a novel model-based gait recognition method, *JointsGait*, which extracts gait information from human body joints. Early gait recognition methods are mainly based on appearance. The appearance-based features are usually extracted from human body silhouettes, which is not invariant to changes in clothing, and can be subject to drastic variations, due to camera motion or other external factors. In contrast to previous approaches, *JointsGait* firstly extracted spatio-temporal features using gait graph convolutional networks constructed by 18 2-D joints, which are less interfered by external factors. Then Joints Relationship Pyramid Mapping (JRPM) are proposed to map spatio-temporal gait features into a discriminative feature space with biological advantages according to physical structure and walking habit at various scales. Finally, we research a fusion loss strategy to help the joints features be insensitive to cross-view. Our method is evaluated on large datasets CASIA B. The experimental results show that *JointsGait* achieves the state-of-art performance, which is less affected by the view variations. Its recognition accuracy is higher than lasted model-based method *PoseGait* in all walking conditions, even outperforms most of state-of-art appearance-based methods, especially when there is a clothing variation.

Index Terms—Gait Recognition, Graph Convolutional Networks, Pyramid Mapping

I. INTRODUCTION

Gait recognition, as an emerging biometric recognition technology, aims essentially to discriminate individuals by the way they walk. Unlike other biometric features such as fingerprint, face, iris and palm- print, gait has its unique advantages such as non-contact during acquisition, hard to fake and particularly suitable for long-distance human identification. Therefore, it has bright prospects in visual surveillance, forensic identification and social security.

However, gait recognition suffers from variations such as view, clothing and carrying. In order to improve the stability of the extracted features, some earlier work tried to model a human

body and to capture difference of motion patterns among different subjects [1–3]. The ideas of using the body part motion are straightforward and reasonable. But it is very challenging to locate and track each body part accurately.

Hence, the appearance-based gait recognition methods [4,5] are more popular than the model-based ones in the past two decades, which usually use the human silhouettes (e.g. Fig.1 (b)) obtained from background subtraction as raw input data. These methods can achieve very high recognition rates when there are not obvious variations. However, when human shape changes greatly in practice (e.g. Fig.1 BG and CL), the appearance-based methods' performance may decrease severely. In addition, the recognition accuracy of appearance-based methods depends heavily on the clarity of the silhouettes. If the camera has a certain movement, it is difficult to obtain reliable silhouettes and satisfactory gait recognition results. In contrast, model-based features are based on human body structure and movements, which are not so sensitive to human shape and human appearance relatively (e.g. Fig.1 (d)).

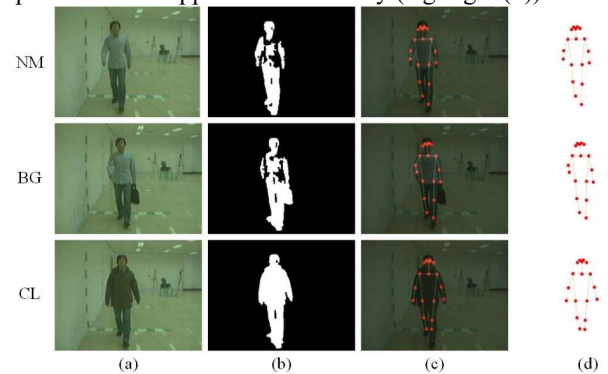


Fig.1. The samples of three common walking conditions. NM is normal, BG is walking with bag, CL is wearing coat or jacket. (a) is original video frames, (b) is silhouettes, (c) is human pose estimation results, (d) is human skeletons.

Recently the progress in human body pose estimation [6] is bring more hope to the model-based methods. Using considerably accurate body joints obtained by pose estimation algorithm as input, this paper presents a new model-based gait recognition method based on gait GCNs, which exploits high-performance gait features from human body structure to handle

many variations. First, we extract spatio-temporal gait features by constructing spatiotemporal joints graphs from video sequence. Second, we propose Joints Relationship Pyramid Mapping (JRPM) to obtain the final feature representation, which maps spatio-temporal gait features into a more discriminative space according to human body structure and walking habit. Third, we research a fusion loss strategy to help the joint features be insensitive to view variations. The advantages of the proposed method are summarized as follows:

Flexible: Unlike the appearance-based methods that use silhouettes as input, our network's input is only 18 2-D joints, which can be estimated from the original video and is not affected by camera movement.

Reasonable: Unlike other spatial pooling methods, our pyramid pooling method inspired by human body structure is more biologically reasonable.

Effective: On popular gait recognition dataset CASIA-B, the proposed model achieves superior performance as compared to previous model-based methods using hand-crafted features or assist of 3D pose information, with considerably less effort in manual design. Experiments show that our model's strong robustness to view and walking condition variations, and its recognition rates could even be comparable with most appearance-based models.

II. RELATED WORK

In this section, we briefly review appearance-based gait recognition methods, model-based gait recognition methods, graph convolutional neural networks and pyramid pooling.

A. Appearance-based methods

Appearance-based gait recognition methods usually use the human silhouettes to extracted different gait features. Some methods contribute to generate different gait template by rendering pixel level operators on the aligned silhouettes in different ways, e.g., Gait energy image (GEI) [4], Chrono-Gait Image (CGI)[7]. In template matching approaches, View Transformation Model (VTM) [8] learns a projection between different views. Stacked Progressive Auto- Encoders (SPA) [9] trying to transform gait images from arbitrary angles to a specific view. View-invariant Discriminative Projection (ViDP) [10] to project the templates into a latent space to learn a view-invariance representation. Recently, some researchers [5,11-14] directly use human silhouettes as input data instead of using gait templates with the help of deep learning methods. The method in [12] is the first one using a deep CNN model to extract feature from human silhouette sequence. GaitSet [5] regards gait as a set consisting of independent silhouettes rather than continuous silhouettes [12], which outperforms the previous state-of-the-art approaches by an outstanding gap.

Although these methods can achieve high accuracy in terms of cross-view condition, they are largely dependent to human appearance and shape which are easily affected by some variations. Besides, their input, silhouettes are also difficult to obtain when the camera moving.

B. Model-based methods

The model-based methods extract features by modeling human body structure and local movement patterns of different body parts. Compared with appearance-based methods, model-based methods can be robust to many variations if human bodies are correctly and high accurately modeled. But it is not an easy task. Therefore, model-based methods are not as popular as appearance-based ones. Some earlier model-based methods even mark different body parts manually. [1] uses a simple stick model to simulate legs and then uses an articulate pendulum movement to simulate the leg movement during walking. Wang et al. [15] argue that the changes of the angle of each joint in temporal domain can be beneficial to recognition. In recent years, some researchers use human body skeleton and body joints to recognize different persons. For example, Kastaniotis et al. [16] use skeleton data from the low-cost Kinect sensor instead of a specific equipment in [2]. It shows that the body joints from Kinect contains enough information for human identification. But in video surveillance, the commonly used cameras are mostly RGB ones, not Kinect sensors.

Recently, as human body pose estimation has achieved great progress, [17] proposes a model-based gait recognition method with 3-D human body joints and human prior knowledge. Although this model is different from the previous methods of marking human body parts by manual methods or special equipment, it still manually defined gait features. Besides, in order to deal with the problem of view changes, it converts 2-D joint points into 3-D joint points, which has a heavy computational cost. However, our method exploits reliable gait features using only 2-D joints with considerably less effort in manual design and has excellent performance.

C. Graph convolutional neural networks

Recent advancements in deep neural networks have led to the development of graph convolutional networks (GCNs) to understand the form of graph structures [18-22]. GCNs generalize convolutional neural networks (CNNs) from low-dimensional grids of images to high-dimensional domains represented by arbitrarily structured graphs. These tasks are categorized into two main categories: spectral perspective and spatial perspective methods. Spectral perspective methods convert graph data into a spectrum and apply CNNs to the spectral domain [18-19]. Different from the spectral perspective methods, spatial perspective methods directly use graph convolutions to define parameterized filters [20-22]. The convolution operation in the spatial perspective resembles the convolution operation on images. This work follows the spatial perspective method.

D. Pyramid Pooling

In many computer vision tasks, in order to help the deep network focus on features with different sizes to gather both local and global information, many methods use pyramid pooling instead of simple global pooling. Spatial Pyramid Pooling network (SPP)[23] maintains spatial information by pooling in local spatial bins, which can improve the

performance of classification and object detection tasks. Similarly pyramid pooling module is also used in [24], the pyramid level pooling separates the feature map into different sub-regions and forms pooled representation for different locations. Horizontal Pyramid Pooling (HPP) [25] horizontally slice the deep feature maps into multiple spatial bins using various pyramid scales in person re-identification task.

Considering the advantages of pyramid pooling and the physiological connection between human body joints, this paper divides the spatio-temporal gait features into different body sub-regions according to the structure of human body and walking habit.

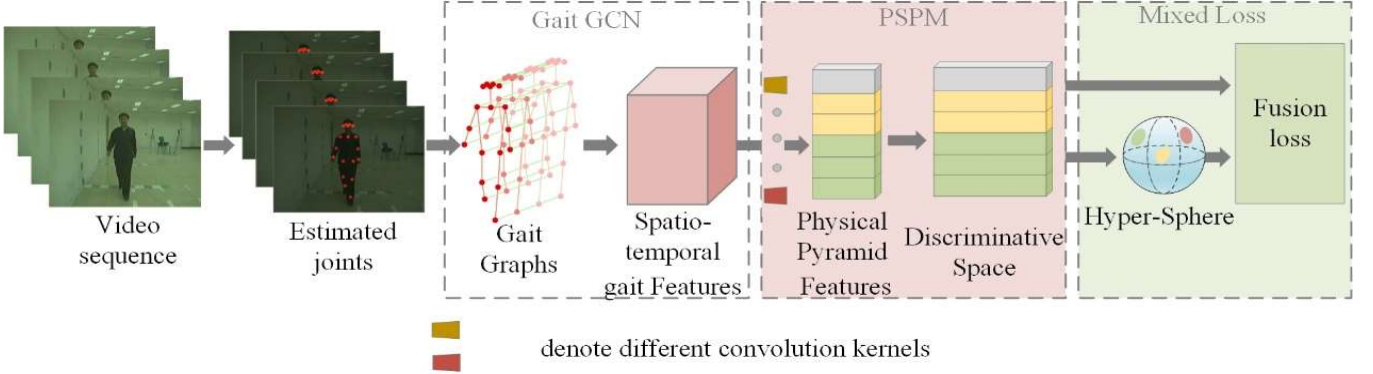


Fig. 2. The framework of the proposed method. Human body joints estimated from video sequence is used to build gait graphs. Through gait graph convolutional networks, spatio-temporal gait features are extracted, which is mapping into discriminative space by JRPM. A fusion loss strategy is applied to optimize our method.

A. Gait Graph Convolutional Networks

1) Gait Graphs

We use all the human joints in a video sequence obtained from pose estimation method *Openpose* [6] to create gait graph structure. The raw skeleton data in one frame produces 18 joints, which are provided as a sequence of vectors. Each vector represents the 2-D coordinates of the corresponding human joint. We employ a spatiotemporal graph to model the structured information among these joints along both the spatial and temporal dimensions. The structure of the graph follows the work of ST-GCN [26]. The left sketch in Fig. 3 presents an example of the constructed gait graphs, where the joints are represented as spatial edges (the red lines in Fig. 3, left). For the temporal dimension, the corresponding joints between two adjacent frames are connected with temporal edges (the green lines in Fig. 1, left). The coordinate vector of each joint is set as the attribute of the corresponding joint.

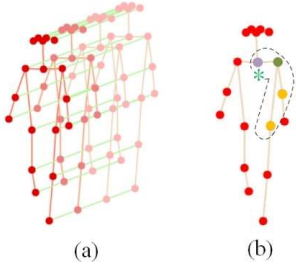


Fig. 3. (a) Illustration of the spatiotemporal gait graphs. (b) Illustration of the mapping strategy. Different colors denote different subsets.

III. THE PROPOSED METHOD

In this section, we describe our method for learning discriminative gait information from human body structure and movements instead of human shape and human appearance, and the overall pipeline is illustrated in Fig. 2. The proposed method takes estimated human body joints as input, next constructs gait graph convolutional networks to extract spatio-temporal gait features, then uses our JRPM to map spatio-temporal gait features into a more discriminative space, eventually handles variations better with the help of a fusion loss strategy. The implementation details are described in the following parts of this section.

2) Graph convolution

Given the graph defined above, multiple layers of spatiotemporal graph convolution operations are applied on the graph to extract the high-level features.

In the spatial dimension, the graph convolution operation on vertex v_i is formulated as Eq. 1:

$$f_{out}(v_i) = \sum_{v_j \in B_i} \frac{1}{Z_{ij}} f_{in}(v_j) \cdot \omega(l_i(v_j)) \quad (1)$$

where f_{in} and f_{out} are the input and output feature map, respectively. B_i denotes the sampling area of the convolution for v_i , which is the 1-distance neighbors of the target vertex (v_i). w is the weight function which provides a weight vector to compute inner product with the input feature map. Note that the number of weight vectors of convolution is fixed, while the number of vertices in B_i is varied. l_i is a mapping function, which is designed to map each vertex with a unique weight vector. Fig. 3 (b) shows this strategy, where $*$ represents the center of gravity of the skeleton, and B_i is the area enclosed by the curve. In detail, the strategy naturally divides B_i into three subsets: S_{i1} is the vertex itself (the green circle in Fig. 3 (b)); S_{i2} is the centripetal subset, which contains the neighboring vertices that are closer to

the gravity center (the purple circle in Fig. 3 (b)); S_{i_3} is otherwise centrifugal subset (the orange circle in Fig. 3 (b)). Z_{ij} is used as the normalizing term to balance the contribution of each subset.

3) Implementation

We implement the graph convolution in spatiotemporal gait graphs to extract the spatio-temporal gait features. The feature map of our network is a $N \times C \times T$ tensor, where N denotes the number of vertexes in video sequence, C denotes the number of channels and T denotes the temporal length. Then Eq. 1 is transformed into

$$\mathbf{f}_{out} = \sum_k^{K_v} \mathbf{W}_k (\mathbf{f}_{in} \mathbf{A}_k^{-\frac{1}{2}} \mathbf{A}_k \mathbf{A}_k^{-\frac{1}{2}}) \odot \mathbf{M}_k \quad (2)$$

where K_v denotes the kernel size of the spatial dimension. With the partition strategy designed above, K_v is set to 3. \mathbf{A}_k is the $N \times N$ adjacency matrix, whose element \mathbf{A}_k^{ij} indicates whether the vertex v_j is in the subset S_{ik} of vertex v_i . $\mathbf{A}_k^{ii} = \sum_j (\mathbf{A}_k^{ij}) + \alpha$ is the normalized diagonal matrix. α is set to 0.001 to avoid empty rows in \mathbf{A}_k . \mathbf{W}_k denotes the weight matrix, where weight vectors of multiple output channels are stacked. \mathbf{M}_k is an $N \times N$ attention map that indicates the importance of each vertex. \odot denotes the dot product.

B. Joints Relationship Pyramid Mapping

JRPM is designed to learn to enhance the discriminative information of partial human skeleton from spatio-temporal gait features, which consists of Joints Relationship Pyramid Pooling (JRPP) and separate fully connect layers (FC).

JRPP is inspired by Horizontal Pyramid Pooling (HPP), which slices the feature maps into multiple scrips in a horizontal manner, and the appearance-based model gaitset [5] uses it to obtain well-performance local features. However, HPP is not suitable for skeleton-based method, because gait graphs constructed by joints are not Euclidean structure. Hence, we propose JRPP to optimize our gait GCNs according to human physical structure, which extracts local gait features according to body parts and walking habit at various scales.

According to different fine-grained body parts, Fig.4 G(1) ~ G(6) shows ways of grouping joints in different scales. The left sketch in Fig.4 shows labels of estimated joints by *openpose*[6]. Especially, 14 and 15 are eyes, 16 and 17 are ears, 0 is nose, and other joints can be seen intuitively. In G(1), the joints with same color or in a same ellipse are divided into a group, and the red square joints are shared by two groups in G(5). Specifically, the whole body in a group in G(1); The upper and lower body are divided into two groups in G(2); In G(3), left arm and right leg are designed in a group according to walking habit, and same for right arm and left leg, because when people walk, they

will naturally swing their arms, which is exactly opposite to the direction of their legs; There are five groups in G(4), and the limbs were divided into four groups; In G(5), the limbs are divided into upper and lower parts, and there are 12 groups in total; Each joint is divided into different groups in G(6).

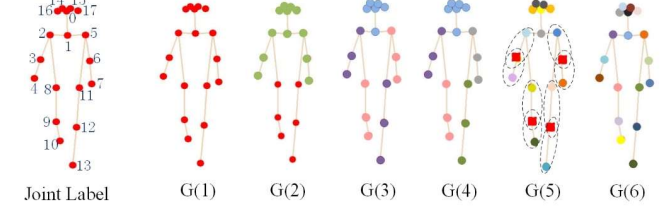


Fig.4. The ways of grouping joints in different scales.

Formally, denote the spatio-temporal gait features extracted by GCNs as F . In Sec. 4.3, we apply JRPP with different pyramid scales on F , and we can find that JRPM reaches the best performance with three pyramid scales. From experiment results. Hence, as shown in Fig.5 we adopt 3 pyramid scales within JRPP. Assume each feature group as $F_{i,j}$, i, j stand for the index of scale and the index of group in each scale. The size of $F_{i,j}$ is $N \times C \times J_{i,j} \times T$, $J_{i,j}$ is the number of joints in the group. For instance, $F_{3,1}$ means the first group in third pooling scale. Then, we pool each feature group $F_{i,j}$ by convolution kernel $k_{i,j}$ to generate local feature $P_{i,j}$, $P_{i,j} = F_{i,j} * k_{i,j}$, and the size of $k_{i,j}$ is $J_{i,j} \times T$.

Instead of applying a 1×1 convolutional layer after the pooling, we use independent fully connect layers for each pooled feature to map it into the discriminative space. And we concatenate features of parts at different pyramid scales to form the final feature representation of each video. In this way, the discriminative ability of human gait can be captured from global to local, from coarse to fine.

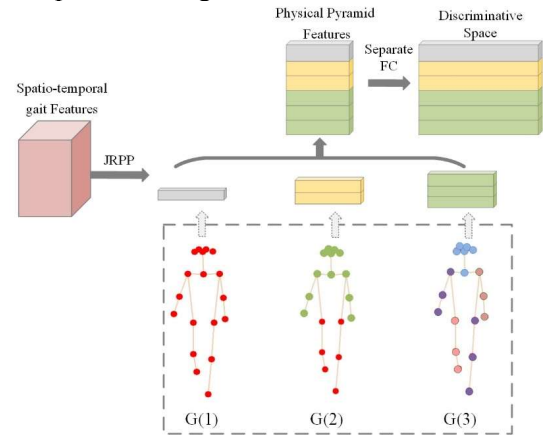


Fig.5. Overview of the proposed JRPM approach. The JRPP is applied on spatio-temporal gait features to produce physical pyramid feature representation of each body part at 3 scales. G(1)~ G(3) are three ways of grouping physical structure in the corresponding scale. Each pooled feature is mapped the discriminative space by separate fully connect layers.

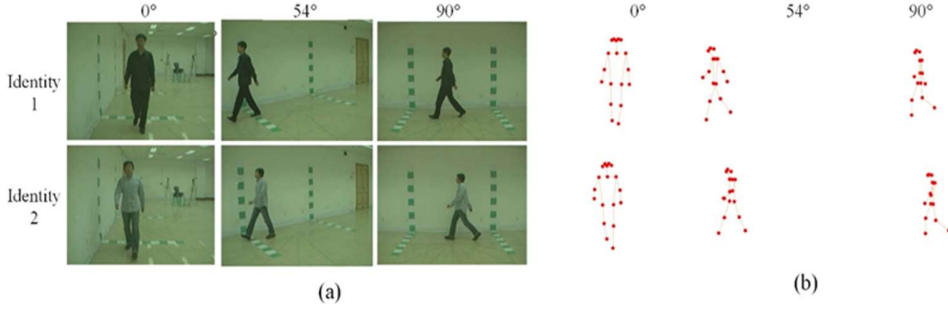


Fig.6. The samples of view variation and the view angles are $\{0^\circ, 54^\circ, 90^\circ\}$. (a) is original video frames (b) is corresponding skeleton data of (a).

C. Fusion loss Strategy

The gait features we get contain both spatiotemporal information and physiological characteristics. However, due to the influence of viewpoints, different viewpoints of the same identity usually have massive visual differences, and it may even be possible that some different identities from the same viewpoints are more similar in vision than the same identity from different viewpoints (e.g. Fig.6.), especially in skeleton data (e.g. Fig.6. (b)). So, we design a fusion loss function to solve the problem of cross-view, that is to reduce the impact of viewpoints when recognizing gait.

We regard different viewpoints of a person as different clusters of a class, so cross-view gait recognition problem can be abstracted as a clustering problem. Therefore, when we design the loss function, we consider two points: 1. The loss function should reduce the intra-class distance and increase inter-class distance. 2. Because the difference of clusters of same class may be very large, it may be difficult to find the cluster center.

Among existing loss functions, the triplet loss [27] is defined as Eq. 3 shows that, given an anchor point x_a , the projection of a *positive* point x_p belonging to the same class y_a is closer to the anchor's projection than that of a *negative* point belonging to another class y_n , by at least a margin m . The advantage of triplet loss is that, while eventually all points of the same class will form a single cluster, they are not required to collapse to a single point; they merely need to be closer to each other than to any point from a different class, which is consistent with our task.

$$L_{tri} = \sum_{\substack{a,p,n \\ y_a=y_p \neq y_n}} [m + D_{a,p} - D_{a,n}]_+ \quad (3)$$

Therefore, we adopt triplet loss to optimize our network at first, and advised in [28], we use improved triplet loss based on batch to accelerate network convergence. We form batches by randomly sampling P classes (person identities), and then randomly sampling K images of each class (viewpoint), thus resulting in a batch of PK images. And we regard different identity at same viewpoints as hard negatives, and same identity at different viewpoints as hard positives. Now, for each sample

a in the batch, we can select the hardest positive and the hardest negative samples within the batch when forming the triplets for computing the loss as shown in Eq. 4

$$L_{tri_BH} = \sum_{i=1}^P \sum_{a=1}^K [m + \overbrace{\max_{p=1 \dots K} D(x_a^i, x_p^i)}^{\text{hardest positive}} - \underbrace{\min_{\substack{j=1 \dots P \\ n=1 \dots K \\ j \neq i}} D(x_a^i, x_n^j)}_{\text{hardest negative}}]_+ \quad (4)$$

where x_j^i corresponds to the j -th feature belongs to the i -th person in the batch.

However, in the real experiment, as shown in Sec. 4.3, we found that although triplet loss can increase inter-class distance and reduce intra-class distance to a certain extent, but the cross-view problem is still difficult for it. So we need another loss function to increase inter-class distance. Arcface loss, as improvement of softmax loss, is proposed to solve face recognition. By mapping features to a hypersphere, inter-class distance can be increased. And its calculation formula is as follows:

$$L_{arc} = -\frac{1}{N} \sum_{i=1}^N \log \frac{e^{s(\cos(\theta_{y_i} + m))}}{e^{s(\cos(\theta_{y_i} + m))} + \sum_{j=1, j \neq y_i}^n e^{s \cos \theta_j}} \quad (5)$$

Where θ is the angle between the feature and the ground truth weight W_y , m is an angular margin penalty, and s is the feature scale.

But arcface loss may also increase intra-class distance because the skeleton data of the same person varies greatly from different viewpoints. Therefore, in order to solve the problem of cross-view, the fusion of triplet loss and arcface loss need to be weighed, the triplet loss should play a major role, and the arcface loss is also indispensable. Finally, we define the loss function of skeleton-based gait recognition as Eq. 6, and in our experiments λ was set to 0.9. It is the best value in our experiments in Sec.4.3.

$$L = \lambda L_{tri_BH} + (1 - \lambda) L_{arc} \quad (6)$$

IV. EXPERIMENTAL RESULTS AND ANALYSIS

A. Datasets and Experimental settings

To evaluate the proposed gait recognition method, RGB color video frames are needed because the human poses should

be estimated from color images and cannot from silhouettes. We chose CASIA B Gait Dataset [29] since it contains the original color video frames. The OUISIR research group in Osaka University [30] and CASIA E [17] also contained the original frames [30]. But they cannot provide because of the privacy issue.

CASIA B dataset is one of the popular public gait datasets widely used in research community. It contains 124 subjects in total (31 females and 93 males). There are 10 sequences for each subject, 6 sequences of normal walking (NM), 2 sequences of walking with bag (BG) and 2 sequences of walking with coat (CL). There are 11 views which were captured from 11 cameras at the same time, the view angles are $\{0^\circ, 54^\circ, \dots, 90^\circ\}$.

As there is no official partition of training and test sets of this dataset, we conduct experiments on two settings which are popular in current literatures. These two settings are named as medium-sample training (MT) and large-sample training (LT). In MT, the first 62 subjects are used for training and the rest 62 subjects are leaved for test. In LT, the first 74 subjects are used for training and the rest 50 subjects are leaved for test. In the test sets of all two settings, the first 4 sequences of the NM condition (NM#1-4) are kept in gallery, and the rest 6 sequences are divided into 3 probe subsets, i.e. NM subsets containing NM #5-6, BG subsets containing BG #1-2 and CL subsets containing CL #1-2.

B. Training And Testing

Training In all the experiments, we use the public available *OpenPose* [6] to estimate the location of 18 joints on every frame of the clips. The mini-batch is composed by the manner introduced in Sec. 3.3 with $P=8$ and $K=16$. We randomly select 120 frames per clips. The gait GCNS model is composed of 9 layers of spatial temporal graph convolution operators. The first three layers have 64 channels for output. The follow three layers have 128 channels or output. And the last three layers have 256 channels for output. The number of scales S in PSPM is set as 4. JRPP pools 256 dimensions spatio-temporal gait features into 256×21 dimensions physical pyramid feature, then maps 512×21 dimensions discriminative space. The margin in BH+ triplet loss is set as 0.2 and the margin in arcface loss is set as 0.35. The models are trained with 2 NVIDIA 1080TI GPUs. we train our model for about 80K iterations.

Testing Given a query \mathcal{Q} , the goal is to retrieve sets with the same identity in gallery set \mathbb{G} . Denote the sample in \mathbb{G} as \mathcal{G} . The \mathcal{Q} is first put into proposed network to generate multiscale features, followed by concatenating all these features into a final representations $\mathcal{F}_{\mathcal{Q}}$ as shown in Fig. 4. The same process is applied on each \mathcal{G} to get $\mathcal{F}_{\mathcal{G}}$. Finally, $\mathcal{F}_{\mathcal{Q}}$ is compared with every $\mathcal{F}_{\mathcal{G}}$ using Euclidean distance to calculate Rank 1 recognition accuracy.

C. Training And Testing

To verify the effectiveness of each component and setting of *JointsGait*, as shown in Table 1, we design several ablation study with different settings on MT, including different loss function strategies, different pyramid scales of JRPM. Note

that all unrelated settings are the same.

TABLE I
ABLATION EXPERIMENTS CONDUCTED ON CASIA-B USING SETTING MT.
RESULTS ARE RANK-1 ACCURACIES AVERAGED ON ALL 11 VIEWS, EXCLUDING IDENTICAL-VIEW CASES.

Strategies		NM	BG	CL
1	Triple loss+ JRPM(1 Scale)	43.76	27.83	22.73
2	Arcface + JRPM(1 Scales)	43.15	29.23	13.67
3	Triple loss+ JRPM(3 Scales)	49.38	32.34	25.68
4	Arcface + JRPM(3 Scales)	51.4	37.1	19.6
5	0.9*Triple loss+0.1* Arcface + JRPM(1 Scales)	53.84	43.19	35.17
6	0.9*Triple loss+0.1* Arcface + JRPM(2 Scales)	68.48	53.25	43.23
7	0.9*Triple loss+0.1* Arcface + JRPM(4 Scales)	71.26	59.27	44.62
8	0.9*Triple loss+0.1* Arcface + JRPM(5 Scales)	71.73	60.43	45.88
9	0.9*Triple loss+0.1* Arcface + JRPM(6 Scales)	70.24	55.83	43.69
10	0.1*Triple loss+0.9* Arcface + JRPM(3 Scales)	58.95	50.83	41.53
11	0.5*Triple loss+0.5* Arcface + JRPM(3 Scales)	63.76	49.83	39.73
12	0.8*Triple loss+0.2* Arcface + JRPM(3 Scales)	70.53	57.40	41.05
13	0.85*Triple loss+0.15* Arcface + JRPM(3 Scales)	71.55	58.11	43.63
14	0.875*Triple loss+0.125* Arcface + JRPM(3 Scales)	72.12	57.69	43.93
15	0.9*Triple loss+0.1* Arcface + JRPM(3 Scales)	73.86	59.14	44.55
16	0.925*Triple loss+0.075* Arcface + JRPM(3 Scales)	72.49	57.85	43.79
17	0.95*Triple loss+0.05* Arcface + JRPM(3 Scales)	68.92	55.82	43.30
18	0.99*Triple loss+0.01* Arcface + JRPM(3 Scales)	68.27	49.91	39.83

Effectiveness of Fusion loss To solve the problem of cross-view, we design a fusion loss function. In order to verify the effectiveness of fusion loss, we set up two groups of experiments to compare the performances of single loss functions and the fusion loss function. In each group of experiments, the pooling method is the same. {row1, row2, row5} is a group, they use pooling method JRPM(1 Scale), that is, global pooling, {row3, row4, row15} is another group, they use pooling method JRPM(3 Scales). From the experimental results, the fusion loss function significantly improves the accuracy of gait recognition than single triple loss or arcface. The reason for this is that due to the skeleton data of the same person varies greatly from different viewpoints, although triplet loss can increase inter-class distance and reduce intra-class distance to a certain extent, the cross-view problem is still difficult for it. Besides, arcface can increase inter-class distance, may also increase intra-class distance.

λ setting Previous analysis shows that the fusion of triplet loss and arcface loss need to be weighed. Because different viewpoints of a person may be very large, it may be difficult to find the cluster center, which is the advantage of triplet loss. Therefore, we consider that the triplet loss should play a major role, and λ should be close to 1. The results of experiments in {row10, ..., row17, row18} have demonstrated this. With the increase of λ from 0.1 to 0.9, the recognition accuracy increases gradually, and then begins to decline. In order to find a more accurate value, we purposely carried out experiments near $\lambda=0.9$, and the highest accuracy was $\lambda=0.9$, so the final setting was $\lambda=0.9$.

Pyramid scales of JRPM {row5, ..., row9, row15} shows the gait recognition accuracy of JRPM with different pyramid scales. From these results, we can find that JRPM reaches the best performance with 3 pyramid scales. Intuitively, the number of pyramid p determines the granularity of the partition feature.

With the number of pyramid scales increasing from 1 to 3, recognition accuracy are significant improved from 53.84% to 73.86% in NM, from 43.19% to 59.14 % in BG, from 35.17% to 44.55% in CL, respectively. The pyramid structure can combine both global and local features, which may increase the discriminative ability of very small partition. However, there is no obvious improvement can be observed in 4 scales, 5 scales and 6 scales. Because more pyramid scales may add redundant information for gait recognition, besides bring additional computational cost. Therefore, we finally adopt 4 pyramid scales in this work. Therefore, we finally adopt 3 pyramid scales in this work.

D. Comparisons with state-of-the-art model-based method *PoseGait*

PoseGait[17] is a state-of-the-art model-based gait recognition method with body pose and human prior knowledge. *PoseGait*[17], as do we, uses *openpose* [6] to obtain 2-D joints, but unlike us, it estimates 3-D joints from the 2-D one to deal with view changes. Then, 3-D joints and three handcrafted features by prior knowledge (joint angle, limb length, joint motion) are concatenated as the input of CNN to recognize gait.

While the proposed method exploits spatiotemporal and physiological gait features for cross-view gait recognition only using 2-D joints with considerably less effort in manual design.

We compare with *PoseGait* [17] on same experimental settings, and its results are directly taken from its original paper. In literature, there are only complete results of experiments on MT, so comparisons of complete experimental results on MT are shown in Fig.7. The average recognition accuracies excluding identical-view cases on two experimental settings (MT and LT) are listed in Table II .

From Fig. 7, it can be found that the proposed method achieves well performance of cross-view recognition than *PoseGait* [17] in all three walking conditions. The cross-view recognition accuracy of the proposed is not only high, but also stable, while *PoseGait* 's [17] accuracy fluctuates greatly, especially when the view difference reaches 90°, *PoseGait* 's recognition accuracy is very low. Therefore, the proposed method can better cope with the view variations than *PoseGait*[17]. And we further compare these two methods in Table II .

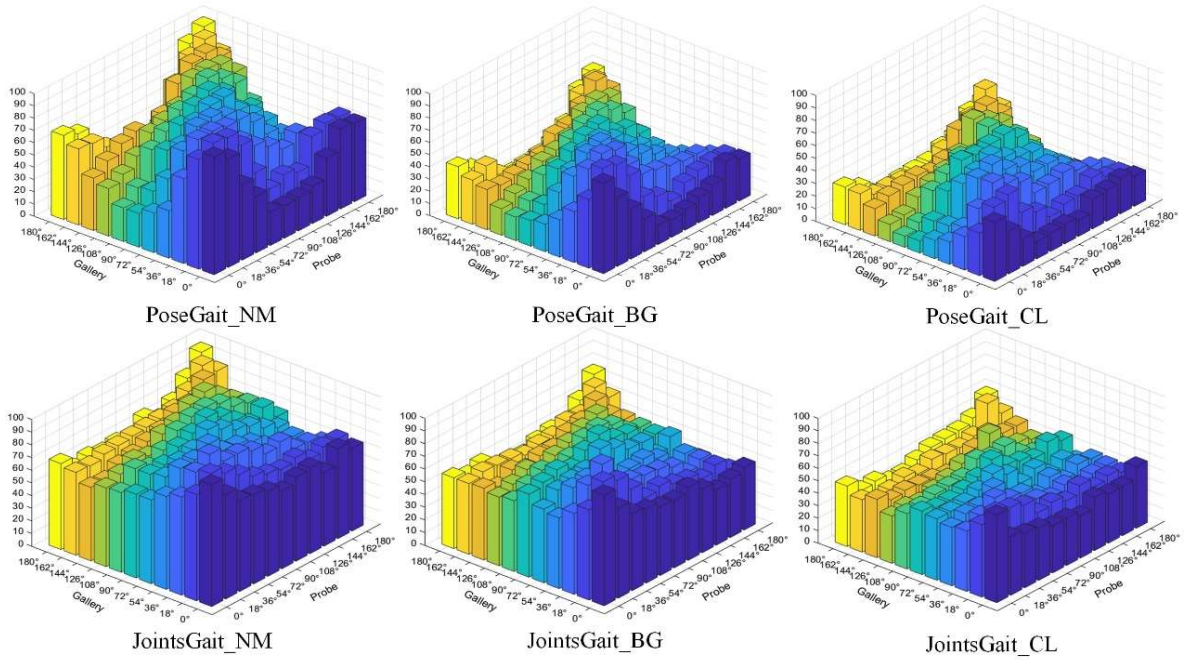


Fig. 7. Complete recognition accuracies (%) comparisons of the proposed method with posegait on MT.

Table II shows average recognition accuracies comparisons of the proposed method with *PoseGait*[17]. All the results are averaged on the 11 gallery views and the identical views are excluded. For example, the accuracy of probe view 0° is averaged on 10 gallery views, excluding gallery view 0°. Then we calculate the mean value (Mean) and standard deviation (Std) of these 11 average recognition accuracies.

As shown in Table II , our method achieves much higher recognition rates of each gallery view than *PoseGait*[17] in all

three walking states of two experimental settings. In MT, the Mean of *JointsGait* is higher than that of *PoseGait*[17] 13.4% in NM, 19.5% in BG, 14.8% in CL. In LT, the Mean of *JointsGait* is higher than that of *PoseGait*[17] 5.8% in NM, 15.7% in BG, 14.6% in CL . That means *JointsGait* is more robust to carrying condition and clothing variation. Besides, *JointsGait* has a much lower Std, which means our method is more robust to view variation.

TABLE II . AVERAGE RECOGNITION ACCURACIES (%) COMPARISONS OF THE PROPOSED METHOD WITH POSEGAIT, EXCLUDING IDENTICAL-VIEW CASES.

Gallery			0°-180°											Mean	Std
Probe			0°	18°	36°	54°	72°	90°	108°	126°	144°	162°	180°		
MT (62)	NM #5-6	PoseGait[17]	48.5	62.7	66.6	66.2	61.9	59.8	63.6	65.7	66.0	58.0	46.5	60.5	7.0
		JointsGait	68.1	73.6	77.9	76.4	77.5	79.1	78.4	76.0	69.5	71.9	64.0	73.9	4.9
	BG #1-2	PoseGait[17]	29.1	39.8	46.5	46.8	42.7	42.2	42.7	42.2	42.3	35.2	26.7	39.6	6.6
		JointsGait	54.3	59.1	60.6	59.7	63.0	65.7	62.4	59.0	58.1	58.6	50.1	59.1	4.2
	CL #1-2	PoseGait[17]	21.3	28.2	34.7	33.8	33.8	34.9	31.0	31.0	32.7	26.3	19.7	29.8	5.3
		JointsGait	41.3	47.6	44.9	44.5	46.3	49.6	47.2	42.6	42.1	42.2	41.8	44.6	2.7
LT (74)	NM #5-6	PoseGait[17]	55.3	69.6	73.9	75.0	68.0	68.2	71.1	72.9	76.1	70.4	55.4	68.7	7.1
		JointsGait	68.8	74.5	76.3	75.1	79	80.2	80.6	77.2	74.6	71.4	61.3	74.5	5.6
	BG #1-2	PoseGait[17]	35.3	47.2	52.4	46.9	45.5	43.9	46.1	48.1	49.4	43.6	31.1	44.5	6.2
		JointsGait	53.2	59.5	63.7	62.0	62.4	64.6	62.9	60.0	60.5	61.8	52.1	60.2	4.1
	CL #1-2	PoseGait[17]	24.3	29.7	41.3	38.8	38.2	38.5	41.6	44.9	42.2	33.4	22.5	35.9	7.5
		JointsGait	45.2	49.6	54.1	55.1	53.8	55.8	54.9	47.8	44.9	50.1	44.0	50.5	4.5

E. Comparisons with state-of-the-art appearance-based methods

As stated in the previous part of the paper, the model-based feature used in the proposed method is compact and has less redundant information as some appearance-based features. It means the feature extraction is more challenging. To show effectiveness of the model-based features, we make comparisons with state-of-the-art appearance-based methods. Especially, *GaitSet*[5] is the appearance-based gait recognition method with the highest recognition rate on at present. Experimental settings are same as in literatures on MT. Except of *JointsGait*, other results are directly taken from their original papers. Average recognition rate comparison results are shown in Table 3, and Fig. 8 is drawn according to Table 3 for

intuitively showing comparisons.

As shown in Table 3, although it is more challenging to compare with state-of-the-art appearance-based methods, our model-based method outperforms most of the advanced appearance-based methods and is second only to *GaitSet*[5]. It is should be noticed that the feature the appearance-based methods used is a kind of appearance-based one which is a high dimension one and we only used 18 body joints as gait feature. Even so, *JointsGait* still achieves satisfactory performance, especially when there is a clothing variation. That means the proposed method is more robust to the clothing variation. It is the advantage of the model-based features. The raw feature is body joints and robust to clothing while the appearance-based features tend to be changed by clothing.

TABLE III AVERAGE RECOGNITION RATE (%) COMPARISONS WITH APPEARANCE-BASED METHODS, EXCLUDING IDENTICAL-VIEW CASES. THE MAXIMUM VALUE IS BOLD, AND THE SECOND LARGEST VALUE IS MARKED WITH BRACKETS.

Gallery NM#1-4			0°-180°											Mean	Std
Probe			0°	18°	36°	54°	72°	90°	108°	126°	144°	162°	180°		
NM #5-6		SPAE[9]	50.0	58.2	61.1	63.3	64.0	62.1	62.3	66.3	64.4	54.5	46.7	59.4	6.3
		Gaitganv1[11]	41.9	53.6	63.0	64.56	63.2	58.1	61.7	65.7	62.7	54.1	40.6	57.2	8.8
		MGAN[13]	54.9	65.9	72.1	74.8	71.1	65.7	70.0	75.6	76.2	68.6	53.8	68.1	7.65
		Gaitganv2[14]	47.1	57.7	66.1	67.4	66.5	61.8	65.0	68.8	66.1	58.2	46.0	61.0	7.99
		GaitSet[5]	86.8	95.2	98.0	94.5	91.5	89.1	91.1	95.0	97.4	93.7	80.2	92.0	5.19
		JointsGait	68.1	73.6	77.9	76.4	77.5	79.1	78.4	76.0	69.5	71.9	64.0	(73.9)	4.9
BG #1-2		SPAE[9]	34.3	41.7	42.0	42.9	46.6	40.0	44.7	45.7	39.6	34.0	32.6	40.4	4.8
		Gaitganv1[11]	28.6	35.2	42.7	34.4	38.0	33.5	36.2	44.8	41.8	33.3	23.6	35.6	5.9
		MGAN[13]	48.5	58.5	59.7	58.0	53.7	49.8	54.0	61.3	59.5	55.9	43.1	54.7	5.63
		Gaitganv2[14]	33.1	38.9	45.7	37.5	40.5	36.3	39.2	47.4	44.6	37.2	28.5	39.0	5.54
		GaitSet[5]	79.9	89.8	91.2	86.7	81.6	76.7	81.0	88.2	90.3	88.5	73.0	84.3	6.13
		JointsGait	54.3	59.1	60.6	59.7	63.0	65.7	62.4	59.0	58.1	58.6	50.1	(59.1)	4.2
CL #1-2		SPAE[9]	21.5	25.4	27.3	28.1	26.9	22.2	22.3	26.3	24.8	21.5	19.6	24.2	2.9
		Gaitganv1[11]	9.8	15.2	24.8	25.0	24.7	19.9	22.7	24.5	27.7	18.0	11.9	20.4	5.9
		MGAN[13]	23.1	34.5	36.3	33.3	32.9	32.7	34.2	37.6	33.7	26.7	21.0	31.5	5.40
		Gaitganv2[14]	11.3	17.2	26.7	27.8	26.4	22.5	24.9	26.5	29.2	19.6	13.3	22.3	6.11
		GaitSet[5]	52.0	66.0	72.8	69.3	63.1	61.2	63.5	66.5	67.5	60.0	45.9	62.5	7.75
		JointsGait	41.3	47.6	44.9	44.5	46.3	49.6	47.2	42.6	42.1	42.2	41.8	(44.6)	2.7

There are two reasons that Our model-based method is inferior to the appearance-based method *GaitSet*[5]. In addition to it uses of high dimensional features, there is another reason that *GaitSet*[5] regards gait as an silhouette image set to enlarge the volume of training data while we use video sequence as input. Therefore, the volume of training data between us varies a lot. Although *GaitSet*[5] has achieved a very high performance in NM, its performance decrease severely in the BG and CL as shown in Fig. 8. This is due to the recognition accuracy of appearance-based methods depends heavily on the clarity of the silhouettes. Besides, if the camera has a certain movement, it is difficult to obtain reliable silhouettes and satisfactory gait recognition results. While *JointsGait* is robust to walking condition changes, which are based on human body structure and movements and are not so sensitive to human shape and human appearance relatively.

Besides, the Std of our model is lowest than other method in almost all experiment settings, including *GaitSet*[5]. That means our method is more robust than these appearance-based methods for cross-view. And an interesting pattern between views and accuracies can be observed clearly in Fig. 8. In these appearance-based methods, besides 0° or 180° , the accuracy of 90° is a local minimum value, which is always worse than that of 72° or 108° , while this case rarely happens in *JointsGait*. The possible reason is that silhouettes likely lose some part of gait information like a left-right swinging of body or arms at 90° view, but the gait graphs constructed by joints can capture this information. However, gait graphs maybe also lose that parallel gait information like stride, so, all methods have minimum value at 0° or 180° view. But the difference between the minimum value of *JointsGait* and the value of other views is very small compared with other methods, which also reflects *JointsGait* is less affected by the view variations.

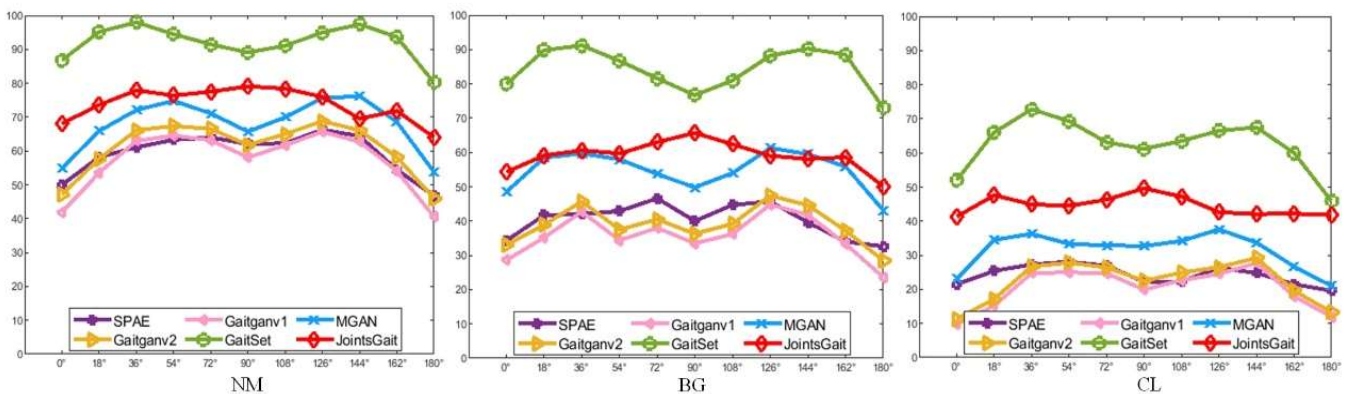


Fig. 8. Average recognition rate (%) comparisons with appearance-based methods, excluding identical-view cases.

V. CONCLUSIONS AND FUTURE WORK

With the progress on human body modeling based on deep learning, in this paper, we proposed a model-based gait recognition method, named *JointsGait*, whose input was only 18 2-D joints rather than silhouettes. Gait GCNs was constructed to extract spatio-temporal gait features from video sequence. Joints Relationship Pyramid Mapping (JRPM) was proposed to map spatio-temporal gait features into a more discriminative biological space according to human body structure and walking habit. A fusion loss strategy was researched to help the final joint features representation to be insensitive to variations. Although it is more challenging to extract gait features because the model-based feature used in the proposed method is compact and has less redundant information as some appearance-based features, the experiments showed that *JointsGait* has received satisfactory performance and could even be comparable with most of appearance-based models, both in cross-view and walking condition variations. It shows that model-based methods have great potential on gait recognition. In the future, we will contribute to large the volume of training data further improve the performance in complex scenarios.

REFERENCES

- [1] M.S. Nixon, J.N. Carter, J.M. Nash, P.S. Huang, D. Cunado, S.V. Stevenage, Automatic gait recognition, in: Motion Analysis and Tracking, 1999, pp. 3/1–3/6.
- [2] R. Tanawongsuwan, A. Bobick, Gait recognition from time-normalized joint-angle trajectories in the walking plane, in: Proceedings of the IEEE Computer Society Conference on Computer Vision and Pattern Recognition, 2001, pp. II–II.
- [3] L. Wang, H. Ning, T. Tan, W. Hu, Fusion of static and dynamic body biometrics for gait recognition, IEEE Trans. Circuits Syst. Video Technol. 14 (2) (2004) 149–158.
- [4] J. Han, B. Bhanu, Individual recognition using gait energy image, IEEE Trans. Pattern Anal. Mach. Intell. 28 (2) (2006) 316–322.
- [5] Chao H, He Y, Zhang J, et al. Gaitset: Regarding gait as a set for cross-view gait recognition[C]//Proceedings of the AAAI Conference on Artificial Intelligence. 2019, 33: 8126-8133.
- [6] Z. Cao, G. Hidalgo, T. Simon, S.-E. Wei, Y. Sheikh, in: OpenPose: realtime multi-person 2D pose estimation using Part Affinity Fields, 2018, pp. 1–14. arXiv: 1812.08008.
- [7] Wang, C.; Zhang, J.; Wang, L.; Pu, J.; and Yuan, X. 2012. Human identification using temporal information preserving gait template. IEEE TPAMI 34(11):2164–2176.
- [8] Han, J., and Bhanu, B. 2006. Individual recognition using gait energy image. IEEE TPAMI 28(2):316–322.

- [9] S. Yu , H. Chen , Q. Wang , L. Shen , Y. Huang , Invariant feature extraction for gait recognition using only one uniform model, *Neurocomputing* 239 (2017) 81–93 .
- [10] Hu, M.; Wang, Y.; Zhang, Z.; Little, J. J.; and Huang, D. 2013. View-invariant discriminative projection for multi-view gait-based human identification. *IEEE TIFS* 8(12):2034–2045.
- [11] Yu S , Chen H , Reyes E B G , et al. GaitGAN: Invariant Gait Feature Extraction Using Generative Adversarial Networks[C]// 2017 IEEE Conference on Computer Vision and Pattern Recognition Workshops (CVPRW). IEEE, 2017.
- [12] Wu, Z.; Huang, Y.; Wang, L.; Wang, X.; and Tan, T. 2017. A comprehensive study on cross-view gait based human identification with deep CNNs. *IEEE TPAMI* 39(2):209–226.
- [13] He, Y.; Zhang, J.; Shan, H.; and Wang, L. 2019. Multi-task GANs for view-specific feature learning in gait recognition. *IEEE TIFS* 14(1):102–113.
- [14] S. Yu , R. Liao , W. An , H. Chen , E.B.G. Reyes , Y. Huang , N. Poh , Gaitganv2: invariant gait feature extraction using generative adversarial networks, *Pattern Recognit.* 87 (2019) 179–189 .
- [15] L. Wang , H. Ning , T. Tan , W. Hu , Fusion of static and dynamic body biometrics for gait recognition, *IEEE Trans. Circuits Syst. Video Technol.* 14 (2) (2004) 149–158 .
- [16] D. Kastaniotis , I. Theodorakopoulos , S. Fotopoulos , Pose-based gait recognition with local gradient descriptors and hierarchically aggregated residuals, *J. Elec- tron. Imag.* 25 (6) (2016) 063019 .
- [17] Liao R, Yu S, An W, et al. A model-based gait recognition method with body pose and human prior knowledge[J]. *Pattern Recognition*, 2020, 98: 107069.
- [18] M. Defferrard, X. Bresson, and P. Vandergheynst. Convolutional neural networks on graphs with fast localized spectral filtering. In *NIPS*, 2016.
- [19] Y. Li, D. Tarlow, M. Brockschmidt, and R. Zemel. Gated graph sequence neural networks. In *ICLR*, 2016.
- [20] Will Hamilton, Zhitao Ying, and Jure Leskovec. Inductive representation learning on large graphs. In *Advances in Neural Information Processing Systems*, pages 1025–1035, 2017. 1, 2
- [21] Federico Monti, Davide Boscaini, Jonathan Masci, Emanuele Rodola, Jan Svoboda, and Michael M. Bronstein. Geometric deep learning on graphs and manifolds using mixture model CNNs. In *Proc. CVPR*, volume 1, page 3, 2017. 1, 2
- [22] Thomas Kipf, Ethan Fetaya, Kuan-Chieh Wang, Max Welling, and Richard Zemel. Neural relational inference for interacting systems. In *International Conference on Machine Learning (ICML)*, 2018. 1, 2
- [23] He, K.; Zhang, X.; Ren, S.; and Sun, J. 2014. Spatial pyramid pooling in deep convolutional networks for visual recognition. In *ECCV*.
- [24] [24] Zhao, H.; Shi, J.; Qi, X.; Wang, X.; and Jia, J. 2017a. Pyramid scene parsing network. In *IEEE CVPR*.
- [25] Fu, Y.; Wei, Y.; Zhou, Y.; Shi, H.; Huang, G.; Wang, X.; Yao, Z.; and Huang, T. 2018. Horizontal pyramid matching for person re-identification. *ArXiv:1804.05275*.
- [26] Yan S, Xiong Y, Lin D. Spatial temporal graph convolutional networks for skeleton-based action recognition[C]//Thirty-second AAAI conference on artificial intelligence. 2018
- [27] Schroff F, Kalenichenko D, Philbin J. Facenet: A unified embedding for face recognition and clustering[C]//Proceedings of the IEEE conference on computer vision and pattern recognition. 2015: 815-823.
- [28] Hermans A, Beyer L, Leibe B. In defense of the triplet loss for person re-identification[J]. *arXiv preprint arXiv:1703.07737*, 2017.
- [29] S. Yu , D. Tan , T. Tan , A framework for evaluating the effect of view angle, clothing and carrying condition on gait recognition, in: 18th International Conference on Pattern Recognition, 2006, pp. 4 41–4 4 4 .
- [30] OU-ISIR Biometric Database. <http://www.am.sanken.osaka-u.ac.jp/BiometricDB/index.html> .



Na Li received her master degree of computer science from Northwestern Polytechnical University (Xi'an) in 2017. She is currently pursuing her Ph.D in Computer Science from school of computer science in Northwestern Polytechnical University. Her research interests primarily lie in visual attention, deep learning and image processing.



Xinbo Zhao received the Ph.D. degree from the Northwestern Polytechnical University, Xi'an, China, in 2003. Currently, he is a professor at the School of Computer Science, Northwestern Polytechnical University. His interests include image processing, computer vision, pattern recognition and artificial intelligence. He is the author or co-author of more than 100 scientific papers.



Chong Ma received his master degree of computer science from Northwestern Polytechnical University (Xi'an) in 2019. He is currently pursuing his Ph.D at school of automation of Northwestern Polytechnical University. His main research interests are deep learning, image processing and human-computer interaction.